Int. J. Heat Mass Transfer. Vol. 32, No. 3, pp. 415–434, 1989
Printed in Great Britain

0017–9310/89 $3.00 + 0.00

Non-isothermal flow of polymers into two-dimensional, thin cavity molds: a numerical grid generation approach

S. SUBBIAH, D. L. TRAFFORD† and S. I. GÜÇERI

Thermal Engineering and Advanced Manufacturing Group, Department of Mechanical Engineering, and Center for Composite Materials, University of Delaware, Newark, DE 19716, U.S.A.

(*Received* 8 *October* 1987 *and in final form* 4 *April* 1988)

Abstract—Flow of polymers into planar mold cavities of irregular shapes is analyzed numerically. The Hele–Shaw approximations are used to simplify the general flow equations which are then solved over the irregularly shaped flow domain using a numerically generated grid. The non-isothermal nature of the flow is modelled, including a temperature and shear-rate dependent viscosity. The temperature distribution in the flow field is calculated using a three-dimensional, transient approach while the prediction of the free surface locations is made using a pseudo steady-state approximation, neglecting the inertial terms. The computational predictions are compared with analytical results and experimental observations indicating good accuracy. The applications of the approach are demonstrated through various examples.

1. INTRODUCTION

THE ABILITY to simulate a realistic mold filling process allows the engineer to optimize the mold design and processing variables. However, the analysis of injection molding processes (often using fiber-filled polymeric suspensions) presents several major challenges. The flow is transient, non-Newtonian and non-isothermal with ongoing solidification as the molten polymer flows through the mold cavity. An important characteristic of the problem is the existence of a continually moving boundary, i.e. the melt front, the location of which is not known *a priori*. Furthermore, the process is highly nonlinear because of the convective terms and the strong dependence of viscosity on the shear rate and temperature. While the fact that most injection molded parts are 'thin walled' allows for an approximation of the flow to a two-dimensional problem, the temperature distribution in the fluid remains fully three-dimensional with significant gradients occurring near the mold walls. In addition, the mold cavities are of irregular shapes and of variable thicknesses requiring the use of a suitable numerical approach for the analysis. The continually changing flow domain also necessitates full or local remeshing to accurately track the flow. This suggests that the mesh generation schemes be highly versatile and computationally efficient.

If fibers are present in the fluid, the resulting fiber orientations significantly affect the microstructure and the resulting thermo-physical properties of the molded part, as well as the possible warpage that can occur during cooling. A chosen method of solution should, therefore, be able to generate the relevant information that can be coupled with fiber orientation studies. The ability to predict the flow characteristics and fiber orientation during injection molding is of interest today.

Considerable progress has been made in the study of polymer flow (in the absence of fibers) in thin cavity molds of irregular shapes. Among others, significant contributions to this problem have been made by Kamal and co-workers [1–5]. In ref. [1] a marker-and-cell computational scheme has been used to model the non-isothermal, viscoelastic polymer flow, taking into account the fountain flow occurring at the melt front. This has been extended to include ongoing solidification next to the mold walls using a non-isothermal crystallization model [2]. This study, however, cannot easily handle molds of irregular geometries. Hieber and Shen [6, 7] have presented a formulation to model non-isothermal, non-Newtonian flows in thin molds of arbitrary geometries by using a hybrid finite-element/finite-difference scheme; but they did not consider the effect of fountain flow at the melt front. Their paper does not include information on the three-dimensional pointwise variation of the temperature field. Couniot and Crochet [8] presented a finite-element based scheme to model the filling of a thin planar mold cavity, without considering the fountain flow effects. The study uses a mesh that has been pre-selected to fill the mold cavity, which is then locally adjusted around the free surface to account for the moving flow front. The stability of Hele–Shaw flows and the wetting layer effect has been investigated by Schwartz [9].

In the present study, a numerical scheme is employed for modelling the mold-filling process with

† Currently with Material Science Corporation, P.O. Box 206, Spring House, PA 19477, U.S.A.

NOMENCLATURE

A_n	exponential term for the temperature dependency of the viscosity model
A, B, C	coefficients used for automatic switching of differencing expressions
c_p	specific heat
h	half gapwidth of mold cavity
i, j, q	nodal indices in the ξ-, η- and z-directions
J	Jacobian of transformation from physical to computational coordinates
k	thermal conductivity
M, N, O	number of nodes in the current mesh in the x- (or ξ), y- (or η), and z-directions, respectively
n	dimensionless power-law index
P, Q	grid control functions
p	pressure
S	measure of fluidity defined in equation (12)
T	temperature
T_w	temperature of the mold wall
T_i	temperature of the fluid at the inlet
t	time
u, v, w	velocities in the x-, y- and z-directions
$\bar{u}, \bar{v}$	velocities in the x-, y-directions averaged through the gapwidth
$\bar{u}_{rel}, \bar{v}_{rel}$	velocities of fluid relative to velocities of the nodes in the x- and y-directions
$\bar{u}_{\xi,rel}, \bar{v}_{\eta,rel}$	velocities of fluid relative to velocities of the nodes in the ξ- and η-directions
x, y, z	coordinate axes of physical domain.

Greek symbols

α_t	thermal diffusivity
$\dot{\gamma}$	shear rate
η_v	kinematic viscosity
η_0	zero-shear-rate viscosity
η_∞	infinite-shear-rate viscosity
λ	time constant used in the Carreau model
ξ, η	coordinate axes of the computational domain
ρ	mass density
Φ	viscous dissipation
ψ	stream function.

non-isothermal, non-Newtonian polymers, partially taking into account the effect of the fountain flow on the temperature field. The analysis is based on a numerical grid generation scheme that facilitates solutions over arbitrarily shaped mold cavities. This approach numerically maps the irregular shape of the flow field to a more regular shape in a computational domain where the governing equations are solved using well-developed finite-difference schemes. This requires the specification of only the boundaries of the mold and all the necessary meshes are self-generated to follow the fluid as it fills the mold cavity. The effect of fountain flow at the advancing front on the temperature field is also partially accounted for by appropriate formulation of the energy equation and choice of boundary conditions. The pointwise velocities obtained from this simulation were used in a computational package, FIBOR [10–12], that predicts the orientation of short fibers in dilute suspensions. Sample results of the flow, temperature and fiber orientation predictions are presented. They are seen to compare well with both analytical and experimental results within certain limitations which are discussed.

2. STATEMENT OF THE PROBLEM

The physical nature of the flow during injection molding in thin-walled molds allows for some simplifications of the general flow equations. The Reynolds number (defined with the cavity gapwidth as the characteristic length) is typically very small, indicating that the viscous forces are dominant, and that the inertial forces can be neglected in the momentum equations. Likewise, the flow and the dynamic forces in the gapwise direction can be neglected due to the small thickness of the mold cavity. The fluid can be assumed incompressible during the filling stage. Convection is considered dominant only in the plane of the mold cavity, while conduction is included in all three dimensions.

Figure 1 depicts a mold configuration showing the basic nomenclature and coordinate axes as used in the problem formulation. The assumptions stated above lead to a Hele–Shaw type flow [13, 14], where the velocity component in the z-direction (w) can be neglected, dropping the z-momentum equation. This leaves u and v as functions of x, y, z, and pressure p as a function of x and y only; thus, reducing the flow problem to a two-dimensional one. For thin cavity molds, a fountain flow effect is observed at the moving free surface and the z-direction velocity cannot be neglected in this region. However, Behrens *et al.* [15] and Coyle *et al.* [16] have shown that this region is only of the order of a few gapwidths. Therefore, this effect is ignored in the present model for the flow but is partially accounted for in the temperature field by a proper choice of boundary conditions.

Adopting the coordinate definition as shown in Fig. 1 and following these assumptions, the expressions

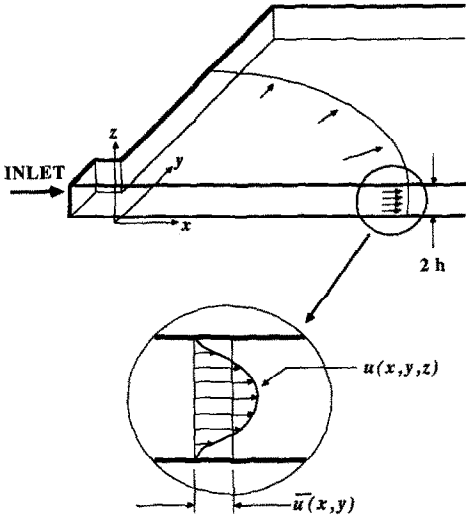

FIG. 1. A Hele–Shaw type flow in a mold cavity of $2h$ gap-width.

that govern the fluid motion become

$$\text{continuity:}\quad \frac{\partial[h\bar{u}(x,y)]}{\partial x}+\frac{\partial[h\bar{v}(x,y)]}{\partial y}=0 \tag{1}$$

$$x\text{-momentum:}\quad -\frac{\partial p(x,y)}{\partial x}+\frac{\partial}{\partial z}\left[\eta_v\frac{\partial u(x,y,z)}{\partial z}\right]=0 \tag{2}$$

$$y\text{-momentum:}\quad -\frac{\partial p(x,y)}{\partial y}+\frac{\partial}{\partial z}\left[\eta_v\frac{\partial v(x,y,z)}{\partial z}\right]=0 \tag{3}$$

where $u(x,y,z)$, $v(x,y,z)$ are the velocity components in the x- and y-directions, and $\bar{u}(x,y)$, $\bar{v}(x,y)$ are the *mean* velocities averaged through the mold cavity gap obtained by

$$\bar{u}(x,y)=\frac{1}{2h}\int_{-h}^{h}u(x,y,z)\,\mathrm{d}z \tag{4}$$

$$\bar{v}(x,y)=\frac{1}{2h}\int_{-h}^{h}v(x,y,z)\,\mathrm{d}z. \tag{5}$$

The assumptions made on the temperature field result in the following energy equation:

$$\rho c_p\left[\frac{\partial T(x,y,z)}{\partial t}+\bar{u}\frac{\partial T(x,y,z)}{\partial x}+\bar{v}\frac{\partial T(x,y,z)}{\partial y}\right]=k\nabla^2T(x,y,z)+\Phi(x,y,z). \tag{6}$$

The Φ term represents the viscous dissipation, which is given by

$$\Phi(x,y,z)=\eta_v(x,y,z)[\dot{\gamma}(x,y,z)]^2=\eta_v\left[\left(\frac{\partial u}{\partial z}\right)^2+\left(\frac{\partial v}{\partial z}\right)^2\right]. \tag{7}$$

The thermophysical properties ρ, c_p and k are maintained constant during the filling process. However, temperature dependency of these parameters can be readily incorporated in the problem formulation in a pointwise manner given the required constitutive equations.

While the Hele–Shaw approximations reduce the flow field to a two-dimensional problem, as defined by equations (1)–(3), the temperature field remains fully three-dimensional, as seen in equation (6). It should also be noted that equation (6) is highly non-linear because of the temperature dependency of the velocity field.

2.1. *Formulation of the problem*

The governing equations presented above can be rearranged into a form that is more suitable for numerical solution [6]. Equations (1)–(3), along with definitions (4) and (5), can be reduced to a single governing equation with either pressure or the stream function as the dependent variable. Expressions for velocities u and v can be obtained by integrating equations (2) and (3) with respect to z and using the following boundary conditions:

$$u=0,\quad v=0\quad \text{for } z=\pm h \tag{8}$$

$$\frac{\partial u}{\partial z}=0,\quad \frac{\partial v}{\partial z}=0\quad \text{for } z=0. \tag{9}$$

This operation yields

$$u(x,y,z)=-\frac{\partial p}{\partial x}\int_z^h\frac{\hat{z}\,\mathrm{d}\hat{z}}{\eta_v} \tag{10}$$

$$v(x,y,z)=-\frac{\partial p}{\partial y}\int_z^h\frac{\hat{z}\,\mathrm{d}\hat{z}}{\eta_v}. \tag{11}$$

Defining a quantity S (a measure of fluidity) as

$$S(x,y)=\int_0^h\frac{z^2\,\mathrm{d}z}{\eta_v} \tag{12}$$

the mean velocities can now be written as

$$\bar{u}=-\frac{S}{h}\frac{\partial p}{\partial x} \tag{13}$$

$$\bar{v}=-\frac{S}{h}\frac{\partial p}{\partial y}. \tag{14}$$

These expressions can be combined with continuity equation (1) to give a unified flow equation in terms of pressure

$$\frac{\partial}{\partial x}\left(S\frac{\partial p}{\partial x}\right)+\frac{\partial}{\partial y}\left(S\frac{\partial p}{\partial y}\right)=0. \tag{15}$$

An equivalent expression can be written in terms of the stream function as the dependent variable by using the definitions

$$\bar{u}=\frac{\partial\psi}{\partial y} \tag{16}$$

$$\bar{v} = -\frac{\partial \psi}{\partial x}. \tag{17}$$

These expressions, when combined with equations (13) and (14) can be substituted into equation (15) to give

$$\frac{\partial}{\partial x}\left(\frac{1}{S}\frac{\partial \psi}{\partial x}\right) + \frac{\partial}{\partial y}\left(\frac{1}{S}\frac{\partial \psi}{\partial y}\right) = 0. \tag{18}$$

In the present study, the stream function formulation is used because of the marginal advantage it has over the pressure formulation in the implementation of the boundary conditions. A normalized stream function is used which is nondimensionalized with respect to the injection velocity and the inlet gate width.

2.2. *Boundary conditions*

Governing equations (15) and (18) are of elliptic type and boundary conditions need to be specified along all the boundaries. For the stream function formulation, the cavity walls represent constant stream function values, with the difference indicating the flow rate. At the inlet of the mold cavity, the derivative of the stream function normal to the inlet plane is set to vanish, following the assumption of uniform velocity at the inlet. At the moving free surface, a zero shear stress condition is applied, leading to another gradient boundary condition here; i.e. the moving front is perpendicular to the streamlines. These boundary conditions can be stated as

$$\psi|_{\text{mold walls}} = \text{constant} \tag{19}$$

$$\left.\frac{\partial \psi}{\partial n}\right|_{\text{inlet, free surface}} = 0. \tag{20}$$

It should be noted here that equation (8) imposes a no-slip boundary condition on the planar top and bottom mold cavity walls, while equation (19) allows for slip along the side walls.

For the temperature field, the fluid at the inlet is held at a constant temperature of T_i and the mold walls are held at T_w. If necessary, spatial and time-dependent variations in the mold wall temperature can be easily incorporated by assigning proper values at each boundary wall node. In addition, the flow configuration and the mold geometries considered in this study lead to a symmetry condition at the mid-plane of the mold cavity. The thermal conditions at the moving front are the least known of all the boundary conditions. Here, the fluid exhibits a 'fountain flow' where the fluid moves away from the mid-plane, towards the top and bottom cavity walls with non-negligible gapwise velocity components. It has been observed [15–17] that this flow convects the fluid from the hot core towards the upper and lower mold walls. A first approximation can be made by setting the fluid along the entire mold mid-plane and the free surface to be equal to the injection temperature of T_i [18]. In the present study, the temperature of the mold mid-plane is evaluated using the symmetry condition. The 'fountain flow' effects at the free surface are partially accounted for by setting the temperature of the flow front to be equal to the temperature of the fluid element at the mid-plane immediately behind the melt front. This boundary condition represents a more realistic behavior and does not impose strong limitations on the free surface temperature as the flow advances in the mold cavity. In a rapid injection operation, the heat loss from the melt front to the ambient is small in comparison with the other heat transfer processes and is neglected. Additional discussions on the boundary conditions at the free surface can be found in refs. [19, 20].

2.3. *Viscosity modelling*

The solution of equations (15) and (18) requires a viscosity model. For a general non-Newtonian fluid, the viscosity depends strongly on the rate of shear as well as the temperature. In the present study, the Carreau model [21] is employed which relates the stress tensor to the rate of shear through the following expression:

$$\eta(\dot{\gamma}) = \eta_\infty + (\eta_0 - \eta_\infty)[1 + (\lambda\dot{\gamma})^2]^{(n-1)/2}. \tag{21}$$

Here, η_0 is the zero-shear-rate viscosity, η_∞ the infinite-shear-rate viscosity, λ a time constant and n the dimensionless power-law index. The temperature dependence can be included [22] as a first approximation by an Arrhenius type relation given as

$$\eta_v = \eta(\dot{\gamma}) \exp\left[-\frac{A_n(T - T_0)}{T_0}\right]. \tag{22}$$

In this expression, T_0 is a reference temperature and A_n an empirical constant obtained from experimental observations over a range of temperatures and shear rates.

3. NUMERICAL SOLUTION PROCEDURE

During the filling process, the flow domain takes on various arbitrary shapes and the solution of the governing equations and their associated boundary conditions over these irregular shapes makes the use of a numerical scheme essential. In similar studies [7, 8] finite-element techniques have been used on a mesh that has been pre-selected to contain the entire mold cavity and the free surface locations are determined at various times during fill by an interpolation procedure. In the current study, meshes are generated at each time step to contain only the fluid domain. This obviates the need for interpolation to locate the free surface.

3.1. *Grid generation*

Numerical grid generation on any irregularly shaped geometry is performed by essentially mapping the boundaries of the body to a more regular shape in a computational domain. A mesh is created on the

transformed, simpler domain and this can then be mapped back to provide a curvilinear mesh on the original irregular shape. The governing equations are similarly transformed and solved on the computational domain, using the well-established finite-difference techniques, and the solutions at every node mapped back onto the physical domain. This technique has been studied and applied to a large number of engineering problems recently and the details of the method can be found in several references including those reported by Thompson and co-workers [23–26], Häuser and Taylor [27] and Güçeri and co-workers [20, 28–30].

Figure 2 illustrates the mapping process and the associated meshes in the physical and computational domains. Note that the transformation need not be performed in the gapwise z-direction if the mold gap-width h remains constant. This allows for a quasi three-dimensional mapping from x, y, z coordinates to ξ, η, z coordinates where the z-axis remains normal to the ξ–η plane and the gapwise discretization of the mold cavity is done in a plane-parallel fashion [28, 30, 31].

While several expressions are possible, Poisson type elliptic expressions are most commonly used to relate the physical (x, y) coordinates to the computational (ξ, η) coordinates due to their inherent 'smoothness' and ability to handle boundary discontinuities. These relations are given as

$$\frac{\partial^2 \xi}{\partial x^2} + \frac{\partial^2 \xi}{\partial y^2} = P \tag{23}$$

$$\frac{\partial^2 \eta}{\partial x^2} + \frac{\partial^2 \eta}{\partial y^2} = Q. \tag{24}$$

This mapping produces a curvilinear mesh over the physical domain in such a way that the boundaries of the physical domain, including the moving flow front, coincide with one or more of the computational coordinate lines. This simplifies the implementation of the free surface boundary conditions without interpolation, and allows the user to monitor smooth advance of the melt front, avoiding the jagged free surfaces that can be seen in some finite-element approaches. In the above equations, P and Q are the grid control functions that can be used to specify mesh concentration in desired areas [24, 26]. Setting $P = 0$ and $Q = 0$ results in a globally uniform mesh and, for the examples considered in the present study, this was adequate to produce good accuracy. An example using grid control in a similar polymer processing problem is reported in ref. [20].

Since the transformation uses second-order partial derivatives, the mapping has to be performed numerically and it is convenient to interchange the dependent/independent variables of equations (23) and (24) to give

$$\alpha x_{\xi\xi} - 2\beta x_{\xi\eta} + \gamma x_{\eta\eta} + J^2(P x_\xi + Q x_\eta) = 0 \tag{25}$$

$$\alpha y_{\xi\xi} - 2\beta y_{\xi\eta} + \gamma y_{\eta\eta} + J^2(P y_\xi + Q y_\eta) = 0 \tag{26}$$

where α, β, γ are the geometric coefficients and J is the two-dimensional transformation Jacobian given by

$$\alpha = x_\eta^2 + y_\eta^2$$

$$\beta = x_\xi x_\eta + y_\xi y_\eta$$

$$\gamma = x_\xi^2 + y_\xi^2$$

$$J = x_\xi y_\eta - x_\eta y_\xi.$$

Central differencing of equations (25) and (26) yields a coupled pair of difference expressions which are then solved to obtain the location of the mesh nodes, $x_{i,j}$ and $y_{i,j}$. The procedure requires only the specification of the fluid boundaries, i.e. the inlet gate,

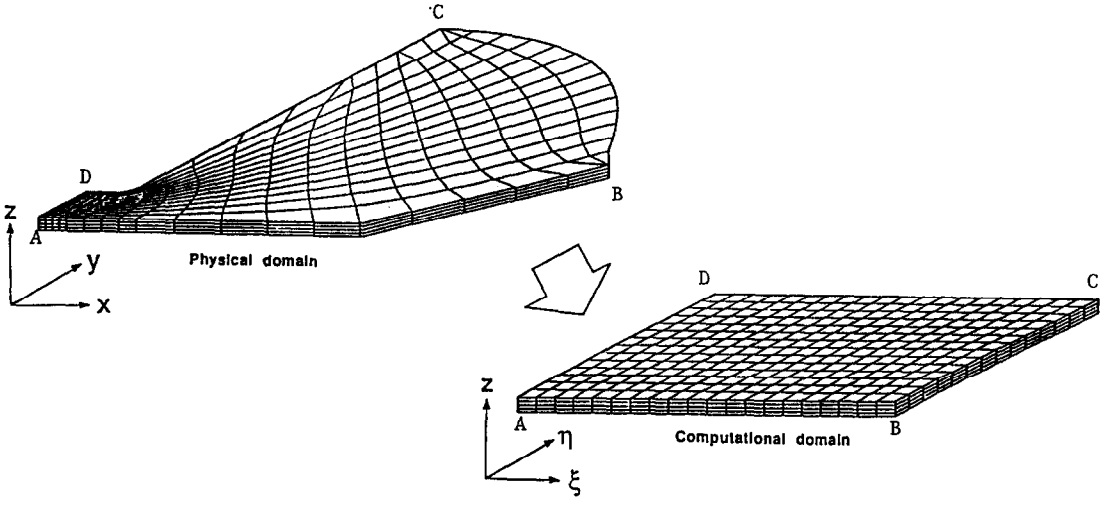

FIG. 2. The numerical mapping of the irregular fluid domain (from the physical x, y, z coordinates) to a more regular computational domain (in the ξ, η, z coordinates).

the mold side walls touched by the fluid and the free surface. To initialize the problem, a finite fluid domain is assumed in the inlet runner on the verge of entering into the mold cavity as shown in Fig. 3. Given a set of user-input nodes to specify the mold boundaries, the flow problem is solved for every time step, the free surface is relocated accordingly and a new mesh is generated over the current flow domain. For small time steps, each new mesh is only marginally different from the previous one and using the previous mesh as the initial guess results in rapid mesh generation.

During the filling process, the flow domain continuously expands. A constant mesh size to cover this domain at all stages of fill could result in either too coarse meshes over large domains (producing unsatisfactory solutions) or in too fine meshes over small domains (poorly utilizing computational resources). Allowing the mesh size to be continuously expanded, as the fluid fills the mold, produces meshes of desired density in a computationally economic way. This is implemented by adding a new curvilinear computational coordinate line to the flow domain each time the free surface passes a mold boundary node.

3.2. *Transformation of the governing equations*

In order to compute finite-difference solutions to the governing equations (18) and (6) over the transformed domain, they need to be expressed in terms of the transformed coordinates ξ, η, and z. Based on the coordinate transformation described above, the flow equation (18) can be expressed as the following elliptic, quasi-linear partial differential equation:

$$\alpha\left[\frac{\partial(1/S)}{\partial\xi}\frac{\partial\psi}{\partial\xi}\right]-\beta\left[\frac{\partial(1/S)}{\partial\xi}\frac{\partial\psi}{\partial\eta}+\frac{\partial(1/S)}{\partial\eta}\frac{\partial\psi}{\partial\xi}\right]+\gamma\left[\frac{\partial(1/S)}{\partial\eta}\frac{\partial\psi}{\partial\eta}\right]+\frac{1}{S}\left[\alpha\left(\frac{\partial^2\psi}{\partial\xi^2}\right)-2\beta\left(\frac{\partial^2\psi}{\partial\xi\partial\eta}\right)+\gamma\left(\frac{\partial^2\psi}{\partial\eta^2}\right)+J^2P\left(\frac{\partial\psi}{\partial\xi}\right)+J^2Q\left(\frac{\partial\psi}{\partial\eta}\right)\right]=0. \quad (27)$$

The Dirichlet boundary conditions for the stream function along the cavity walls remain unchanged, while the Neumann boundary conditions at the cavity inlet and the moving front are now expressed as

$$\alpha\frac{\partial\psi}{\partial\xi}-\beta\frac{\partial\psi}{\partial\eta}=0. \quad (28)$$

Following the definition of stream function in the computational domain, the expressions for $\bar{u}$ and $\bar{v}$ components of velocity along the free surface can be obtained as

$$\bar{u}=\frac{1}{J}\left[\frac{\partial x}{\partial\xi}\frac{\partial\psi}{\partial\eta}-\frac{\partial x}{\partial\eta}\frac{\partial\psi}{\partial\xi}\right] \quad (29)$$

$$\bar{v}=\frac{1}{J}\left[\frac{\partial y}{\partial\xi}\frac{\partial\psi}{\partial\eta}-\frac{\partial y}{\partial\eta}\frac{\partial\psi}{\partial\xi}\right]. \quad (30)$$

Equation (27) can be solved at every time level to obtain the stream function values over the flow domain. Equations (29) and (30) can be then used to increment the location of the free surface for every time step, which is followed by regeneration of the mesh.

The calculation of the temperature field is an initial-value problem. It needs to be evaluated after the free surface has progressed by a small time increment and the new mesh locations have been determined. The motion of the nodes can be incorporated [32] into energy equation (6) by defining

$$\bar{u}_{\text{rel}}=\bar{u}-u_{\text{node}} \quad (31)$$

$$\bar{v}_{\text{rel}}=\bar{v}-v_{\text{node}} \quad (32)$$

where $\bar{u}_{\text{rel}}$ and $\bar{v}_{\text{rel}}$ indicate the relative velocities of the fluid particles with respect to the moving grid points. The transformed energy equation is then

$$\frac{\delta T}{\delta t}+\frac{\bar{u}_{\text{rel}}}{J}\left[\frac{\partial y}{\partial\eta}\frac{\partial T}{\partial\xi}-\frac{\partial y}{\partial\xi}\frac{\partial T}{\partial\eta}\right]+\frac{\bar{v}_{\text{rel}}}{J}\left[\frac{\partial x}{\partial\xi}\frac{\partial T}{\partial\eta}-\frac{\partial x}{\partial\eta}\frac{\partial T}{\partial\xi}\right]=\frac{\alpha_t}{J^2}\left[\alpha\frac{\partial^2T}{\partial\xi^2}-2\beta\frac{\partial^2T}{\partial\xi\partial\eta}+\gamma\frac{\partial^2T}{\partial\eta^2}\right]+\alpha_t\frac{\partial^2T}{\partial z^2}+\frac{\eta_t\dot{\gamma}^2}{\rho c_p} \quad (33)$$

The boundary conditions for the energy equation can be expressed as

$$T|_{\text{mold inlet}}=T_{\text{i}} \quad (34)$$

$$T|_{\text{cavity walls}}=T_{\text{w}} \quad (35)$$

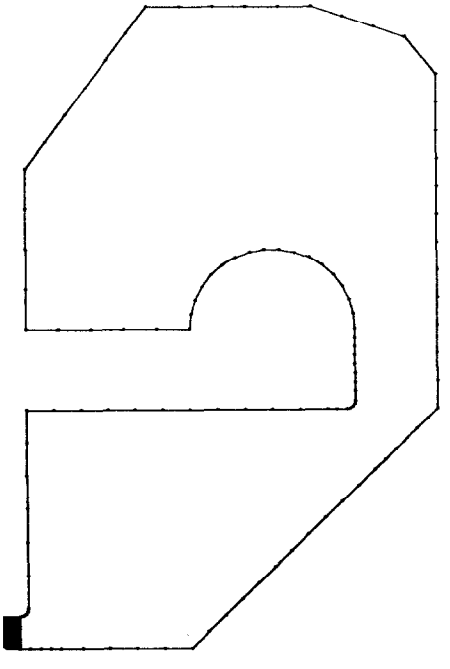

FIG. 3. Problem initialization: the mold shape is specified by user-input nodes along the boundary. An initial fluid domain is assumed in the inlet gate and an initial mesh needs to be generated here by the user.

$$\left.\frac{\partial T}{\partial z}\right|_{\text{mid-plane}} = 0 \tag{36}$$

$$T|_{\text{free surface};M,j,q} = T|_{M-1,j,1}. \tag{37}$$

Note here that i, j, q are the nodal indices in the ξ-, η- and z-directions having maximum values of M, N and O.

3.3. *Discretization*

Since convection is considered to be the dominant mechanism over conduction in the mold plane, the Peclet number for the process is large and upwind differencing is required for stability. The decision on which direction is upstream must be based on the relative velocity of the fluid with respect to the nodes, and not simply the velocity of the fluid, since the nodes are also being relocated. The $\bar{u}_{\text{rel}}$ and $\bar{v}_{\text{rel}}$ need to be transformed to relative velocities in the computational plane along the ξ-direction (i.e. $\bar{u}_{\xi,\text{rel}}$) and along the η-direction (i.e. $\bar{v}_{\eta,\text{rel}}$). These are

$$\bar{u}_{\xi,\text{rel}} = \frac{1}{J}(\bar{u}_{\text{rel}} y_\eta - \bar{v}_{\text{rel}} x_\eta) \tag{38}$$

$$\bar{v}_{\eta,\text{rel}} = \frac{1}{J}(\bar{v}_{\text{rel}} x_\xi - \bar{u}_{\text{rel}} y_\xi). \tag{39}$$

The Appendix details a method for directly using the proper upwind discretization depending upon the magnitude of these relative velocities.

3.4. *Contact point locations*

As stated earlier, a no-slip condition is applied along the top and bottom cavity walls, while a slip condition exists along the mold side walls as a consequence of the Hele–Shaw approximations. Since the mold wall itself is a streamline and because the normal derivative of the stream function along the free surface is set to vanish, as given by equations (19) and (20), it follows that the moving free surface is always normal to the side walls of the mold cavity at the contact points. This is implemented by imposing

$$\frac{\partial \xi}{\partial n} = \frac{1}{J\sqrt{\gamma}}\left[\gamma \frac{\partial \xi}{\partial \eta} - \beta \frac{\partial \xi}{\partial \xi}\right] = 0. \tag{40}$$

It follows that

$$\beta = 0 = x_\xi x_\eta + y_\xi y_\eta. \tag{41}$$

The location of the contact point is determined by expressing equation (41) in finite-difference form (using one-sided three-point differencing for the evaluation of the derivatives) and solving for one of the physical coordinates, say $x_{i,j}$. The value of $y_{i,j}$ then follows the local description of the boundary segment in the form of a local curve fit. If the slope of the boundary segment is infinitely large, then the $x_{i,j}$ value can be set to the x value of the line segment and the y coordinate can be calculated using

$$y_{i,j} = \frac{4y_{i,j-1} - y_{i,j-2}}{3}. \tag{42}$$

This produces a three-point extrapolation of the free surface to meet the mold wall normally. If the free surface approaches a turn in the mold wall such that the mold wall parallels the free surface segment immediately adjacent it, the three-point differencing can produce a contact angle that is not normal to the mold wall. The error associated with this is small and is neglected.

3.5. *Stability*

The stability of a marching scheme directly depends on the selected time increment. Based upon the *Von Neuman* stability analysis [33], a stable time increment for the solution of equation (33) can be formulated as

$$\Delta t \leqslant \left[\frac{2\alpha_t}{(\Delta x)^2} + \frac{2\alpha_t}{(\Delta y)^2} + \frac{2\alpha_t}{(\Delta z)^2} + \frac{\bar{u}}{\Delta x} + \frac{\bar{v}}{\Delta y}\right]^{-1}. \tag{43}$$

It must be noted that the critical time increment must be evaluated at every time step because of the changing mesh configuration. This condition is usually more stringent than the Courant estimation for stable time increments. To be consistent, the time increment for the advancement of the free surface is set to be the same as the time increment used in the energy equation.

3.6. *Solution procedure*

Starting from an initial mesh enveloping the initial fluid domain, the transformed flow equation (27) is solved using an iterative procedure to obtain the stream function solutions over the fluid domain. Using equations (29) and (30), the fluid velocities along the free surface are determined and the free surface is moved to a new location for a small, stable time increment. A new mesh is then generated over the new fluid domain using the previous mesh as a first guess. When the free surface crosses every prespecified point on the mold boundary, the mesh size is enlarged by one more column of nodes in the flow direction. While such an approach helps to keep the mesh size (and hence the computational time) to a minimum, the marching scheme used to calculate the temperature solutions from the transformed energy equation cannot be applied if the mesh has been enlarged. In this case, an extra mesh line is introduced in the old mesh and the necessary parameters are determined by interpolation before proceeding. Since the grid distribution at every time step serves as the initial guess for the grid generation at the next time level, this facilitates the quick generation of a new mesh.

4. SAMPLE RESULTS

In this section, the accuracy of the formulation and the solution technique described above is examined and their applicability to irregularly shaped planar mold cavities is demonstrated.

4.1. *Comparison with analytical solution*

The equations governing the flow can be solved analytically for a simple rectangular cavity to (partially) evaluate the accuracy of the numerical approach. For this purpose, a rectangular mold cavity of $5 \times 2 \times 0.1$ cm is considered. The fluid is injected at a constant injection velocity of 1.0 cm s^{-1}, and is assumed to follow a power-law viscous behavior. An analytical expression can then be obtained for the isothermal flow by integrating equation (2). Assuming h and $\bar{u}$ to be constant, the expression for pressure becomes

$$p = -\int_0^x \frac{h\bar{u}\,dx}{S} = -\frac{\bar{u}\eta_v(2+1/n)^n}{|\nabla\psi|^{1-n}h^{n+1}}\int_0^x dx \quad (44)$$

where

$$\nabla\psi = \left[\left(\frac{\partial\psi}{\partial x}\right)^2 + \left(\frac{\partial\psi}{\partial y}\right)^2\right]^{1/2}. \quad (45)$$

This allows a comparison between the numerical calculations and the analytical solution for various power law indices. The results are presented in Table 1 using a fluid viscosity of 10 poise with a power-law index of $n = 1$, indicating good accuracy for the numerical simulation.

4.2. *Comparison with experimental observations*

A simple laboratory mold was constructed for examining the melt front locations and inlet pressures at various times during the filling operation. Aluminum sheets were cut to form a rectangular mold cavity of dimensions $30.32 \times 20.0 \times 0.3175$ cm, as shown in Fig. 4. The mold was fitted with a grid transparent top through which melt front locations were recorded with a video-camera. The inlet was located at the upper left-hand corner of the rectangular mold cavity and a potentiometric pressure transducer was located there to monitor the injection pressure. A cylinder and piston arrangement was used to inject the fluid at a constant velocity of 3.1 cm s^{-1} at the gate, resulting in a total fill time of 100 s. Experiments were conducted using corn syrup as the working fluid. Its viscosity was measured to be 47.05 poise using a Weissenberg rheogeniometer and it was seen to exhibit a Newtonian behavior over the range of shear rates for the experiment.

Table 1. Comparison of the solutions for inlet pressure when filling a simple rectangular mold using shear-thickening. Newtonian and shear-thinning fluids

	Pressure (analytical) (kPa)	Pressure (numerical) (kPa)	Percentage error (%)
$n = 1.2$	12.7055	12.6792	0.2
$n = 1.0$	6.0000	5.9875	0.2
$n = 0.4$	0.6049	0.6036	0.2

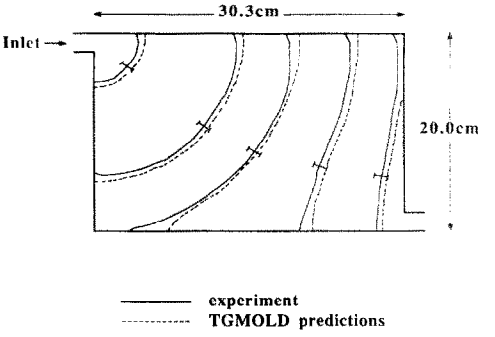

FIG. 4. Comparison of the predictions of the free surface locations with experimental observations at 6.3, 28.0, 52.4, 74.8 and 91.4 s (total fill time = 100 s).

Figure 4 shows the comparison of the predicted and observed free surface locations at various time steps. The gauge pressure measured at the inlet gate at the time of complete fill was 10.55 kPa ($\pm$0.345 kPa) and the numerically predicted value for the same case was 9.69 kPa.

4.3. *Non-isothermal filling of an irregular mold geometry*

Non-isothermal flow is simulated for the mold cavity shown in Fig. 3, where polystyrene is considered as the injected fluid. The mold shape is approximately 5 cm long, 8 cm wide and has a gapwidth of 0.25 cm. A constant flow rate of 3.755 $cm^3\ s^{-1}$ with polystyrene at 290°C is used at the inlet. The mold walls are held at a constant temperature of 85°C. The Carreau coefficients of viscosity for polystyrene are taken (at 453 K) as $\eta_0 = 1.48 \times 10^4$ N s m^{-2}, $\eta_\infty = 0$, $\lambda = 1.04$ s, $n = 0.398$ [34]. The temperature dependency was modelled using $T_0 = 453$ K and $A_n = 0.03$. A sample of the meshes generated during filling is shown in Fig. 5. Note that the nodes specified on the mold boundary have been located such that the resulting meshes during the flow are more concentrated around sharp corners to help avoid instabilities in the calculations. Unusually skewed meshes can result in erroneous temperature predictions and this was continuously monitored during the filling simulation.

At the beginning of injection, a $5 \times 15 \times 10$ mesh was used and this was continuously enlarged to a final mesh size of $64 \times 15 \times 10$ at the instant of complete fill. The time step used was 0.0001 s and the predicted

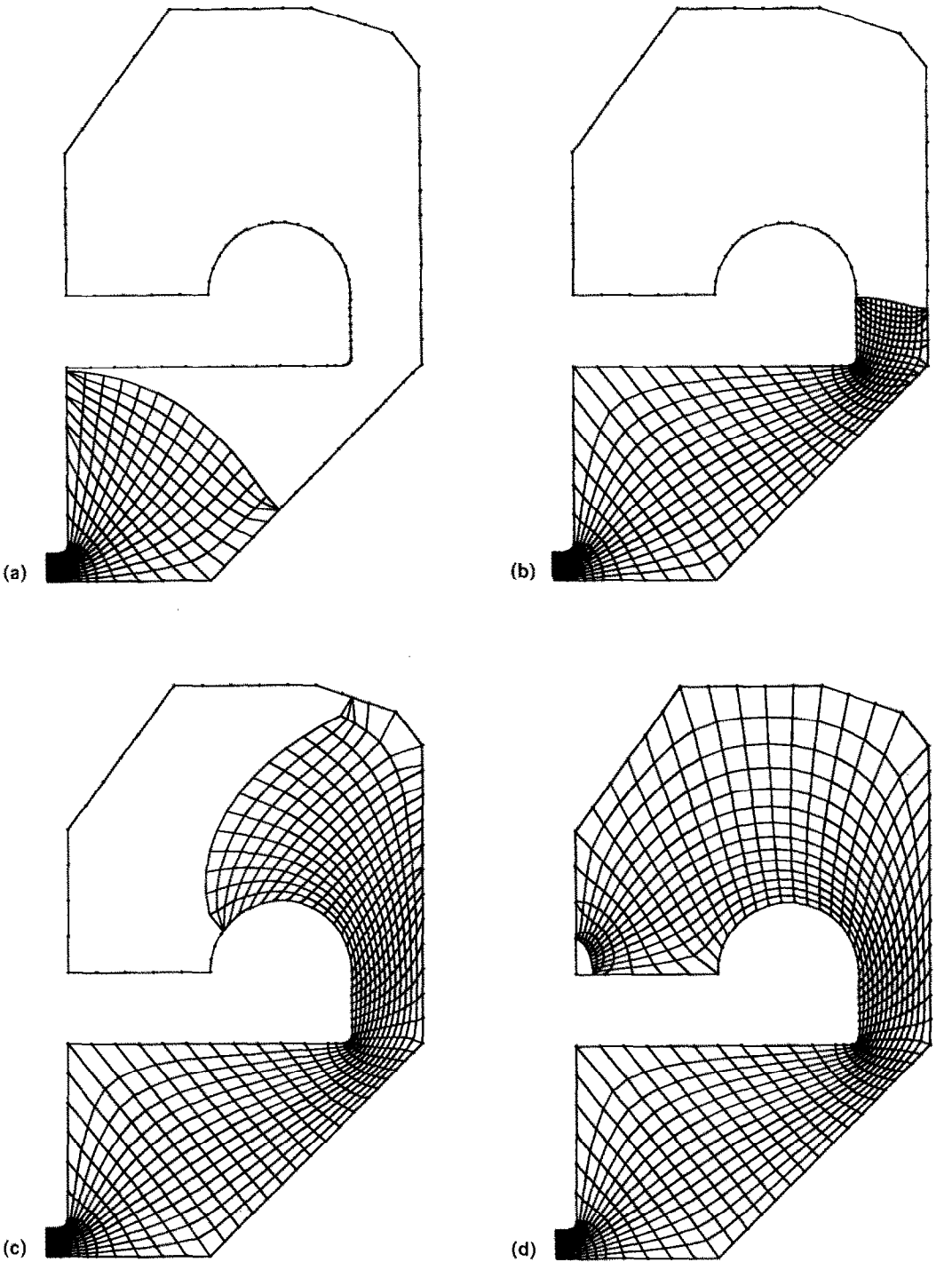

FIG. 5. Irregular mold geometry: the numerically generated meshes over the flow domain at selected times during the filling simulation.

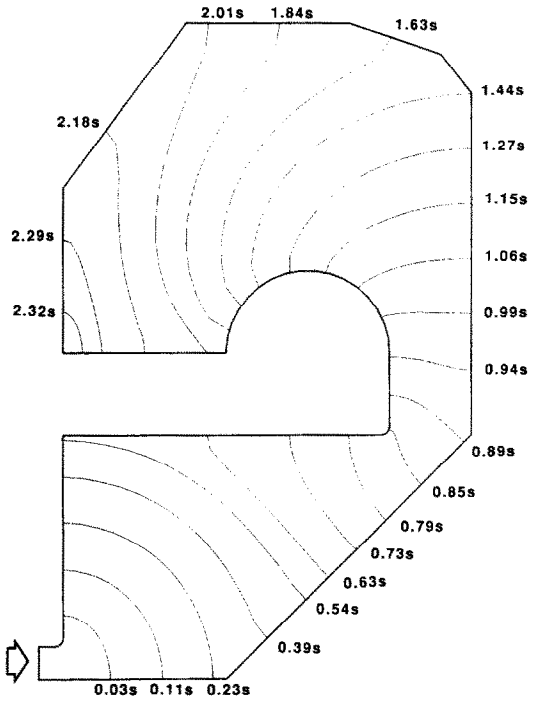

FIG. 6. Irregular mold geometry: the predicted locations of the melt front at selected time steps during the flow.

fill time was 2.32 s. The problem required 8 h and 20 min of CPU time on a VAX 11/785 computer. Figure 6 shows the predicted locations of the polymer front at selected time steps.

A measure of evaluating the accuracy of simulation is the error in predicting the *filled volume* which is defined as

$$\text{error}_{\text{f.v.}} = \frac{\text{Vol}_{\text{numerical}} - \text{Vol}_{\text{exact}}}{\text{Vol}_{\text{exact}}}. \tag{46}$$

This has been evaluated for the irregular mold shape shown here and the resulting error is plotted in Fig. 7. The error is seen to be within acceptable limits. The numerical grid generation approach results in typically less volumetric error as described by equation (46) because the fluid domain is meshed fully without interpolation. A limited comparison of the numerical grid generation scheme presented here and a finite-element approach [35] in modelling a mold filling process is presented in refs. [28, 31], indicating excellent agreement between the two techniques with comparable mesh structures.

The pressure distribution near the completion of the filling stage is shown in Fig. 8. At the instance of mold fill, the pressure in the inlet gate is predicted to be 4413 kPa (640 psig).

The three-dimensional temperature solution is displayed (Fig. 9) as a set of contour plots in the x–y plane for three different heights in the mold gapwidth: (a) the plane immediately below the top mold wall (at $z = 0.1111$ cm); (b) the plane quarter gapwidth deep (at $z = 0.0555$ cm); and (c) the mold mid-plane (at $z = 0$ cm). While the large temperature gradients near the mold walls are clearly seen as expected, the effect of the fountain flow is also seen in Fig. 9(a), where the temperature at the free surface is higher in comparison to its neighboring points due to the fluid being convected up from the warmer mold mid-plane.

The prediction of fiber orientation is of considerable interest. Solution of the continuum equations numerically allows for the recovery of essential

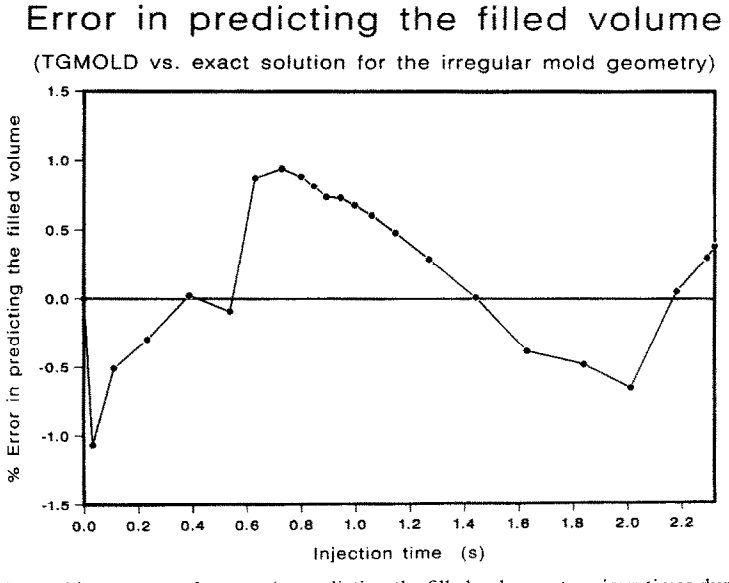

FIG. 7. Irregular mold geometry: the error in predicting the filled volume at various times during the flow.

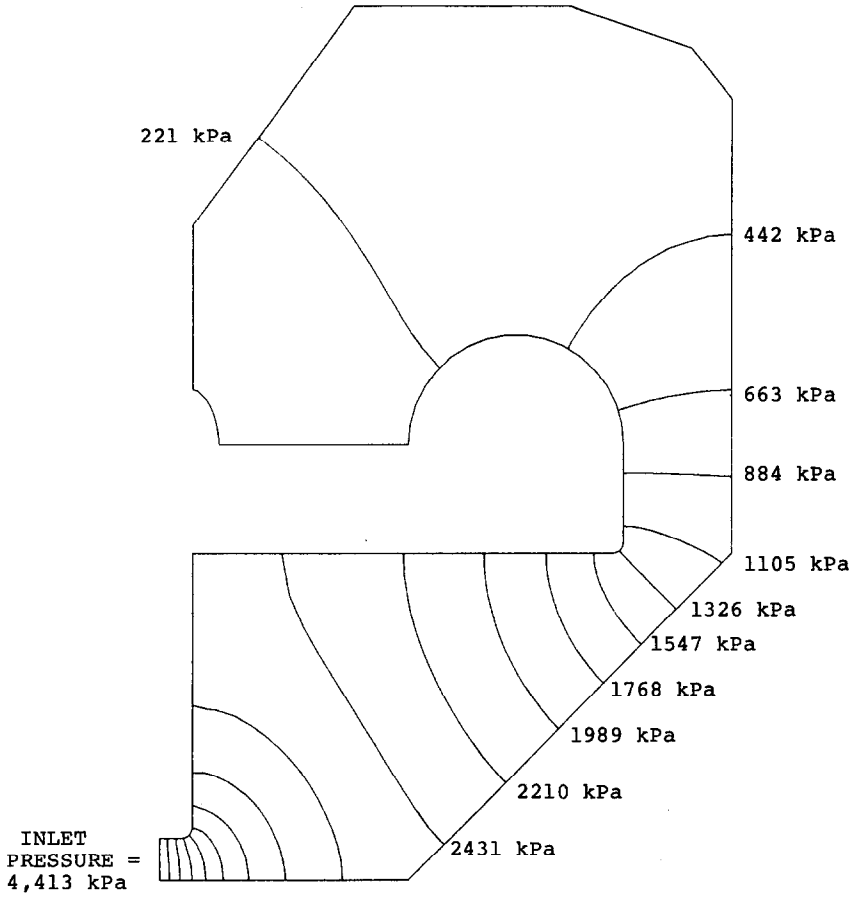

FIG. 8. Irregular mold geometry: prediction of the pressure distribution at the instance of mold fill. Injection pressure at inlet is 4413 kPa (640 psig), each contour corresponds to a step of 221 kPa (32 psi).

flow information to conduct such a prediction as shown in Fig. 10 where the flow studies using TGMOLD [36] are coupled with the fiber orientation predictions using FIBOR [12].

4.4. *Temperature distributions through the mold gapwidth*

The use of a quasi three-dimensional transformation allows the user to gain valuable information about the distribution of the flow variables and temperature in the gapwise direction. To demonstrate this, a $2 \times 6 \times 0.2$ cm rectangular mold cavity is considered. The simulation was performed using polystyrene with injection velocities of 30, 50, 150 and 500 cm s^{-1}. The injection temperature is taken as 290°C, while the mold walls are maintained at 85°C. The problem is solved on the half gapwidth ($z = 0$–h) by discretizing the half gap into nine plane-parallel zones of equal thickness. The simulation of this process was computed in 133 s on a VAX 11/785 computer, and in 14.2 s on an ALLIANT FX-80 parallel computer. Figure 11 shows the distributions of the temperature in the z-direction. As expected for high injection rates, the temperatures are seen to exceed the inlet temperature due to shear heating during the flow. The viscosity distribution across the gap is depicted in Fig. 12 showing the large variations due to the strong temperature and shear rate dependence of the fluid. Figure 13 shows the velocity distributions in the half gap for various fill rates.

The gapwise temperature distribution along the centermost curvilinear coordinate ($\eta = N/2$) is shown in Fig. 14. The simple boundary condition used at the free surface for the temperature is seen to effectively predict the convective nature of the fountain flow. This result compares well qualitatively with the results presented by Hieber in ref. [19].

5. CONCLUSION

A numerical grid generation approach to the analysis of injection molding processes is presented. The technique is shown to have the ability to account for the irregularly shaped two-dimensional nature of the flow field and the three-dimensional nature of the temperature field. The technique is particularly advan-

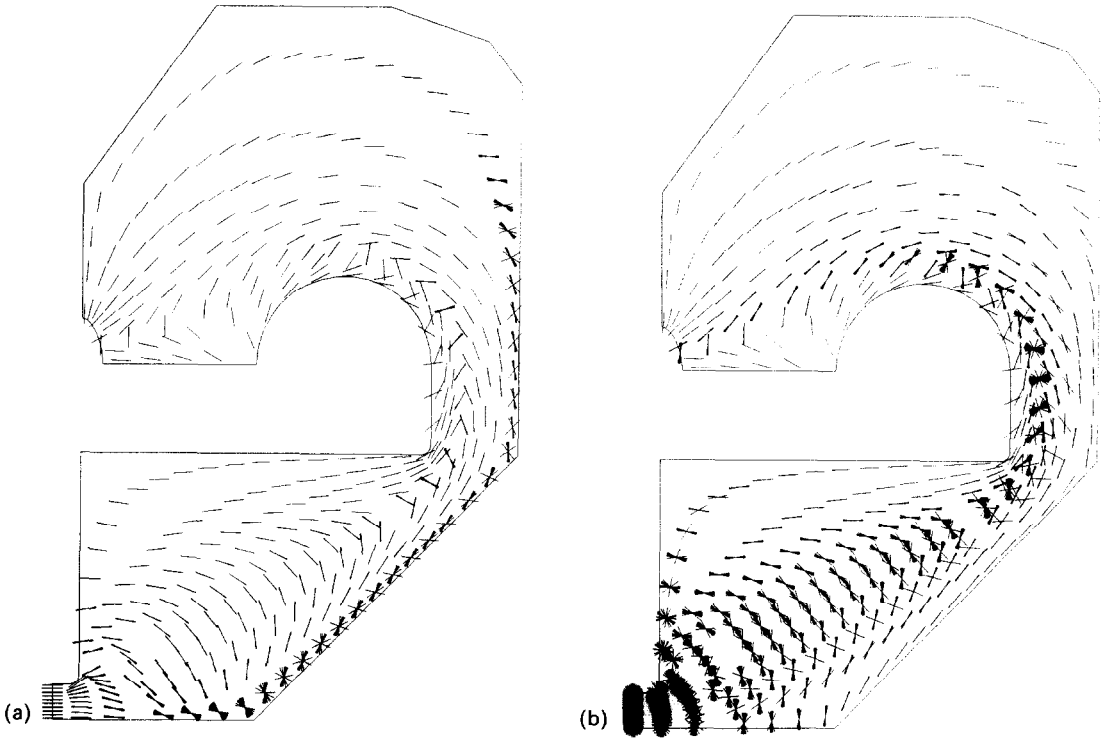

FIG. 10. The predicted fiber orientations at fill by FIBOR (a) for fibers aligned with the flow at the inlet and (b) for fibers randomly aligned in the flow at the inlet.

tageous in implementing the various boundary conditions and in tracking the continuously deforming melt front without interpolation. Since the technique self-generates all the required meshes for a given mold geometry, it requires little startup effort from the user. The non-isothermal nature of the flow has been modelled and the effects of shear heating are clearly seen in the predictions. A simple but effective formulation has been used to include the convective effect of the fountain flow on the temperatures near the melt front. The method described in this paper has been developed into a code (TGMOLD) [36].

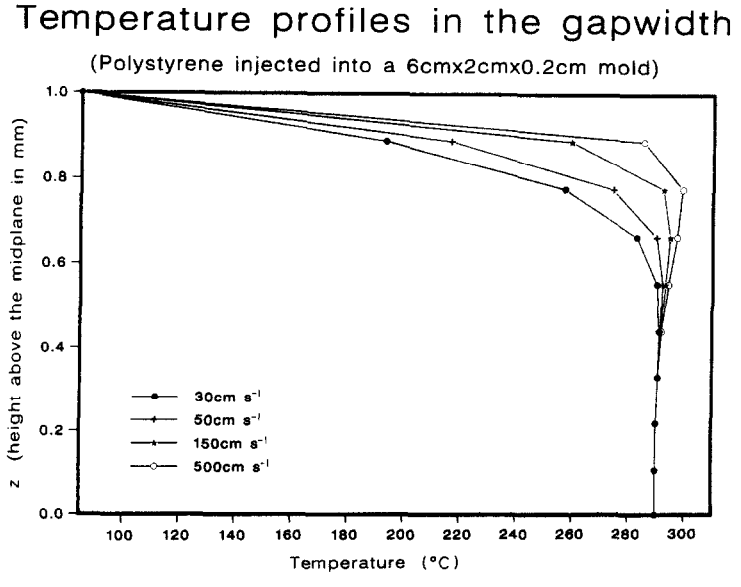

FIG. 11. The gapwise temperature distribution in a rectangular mold cavity.

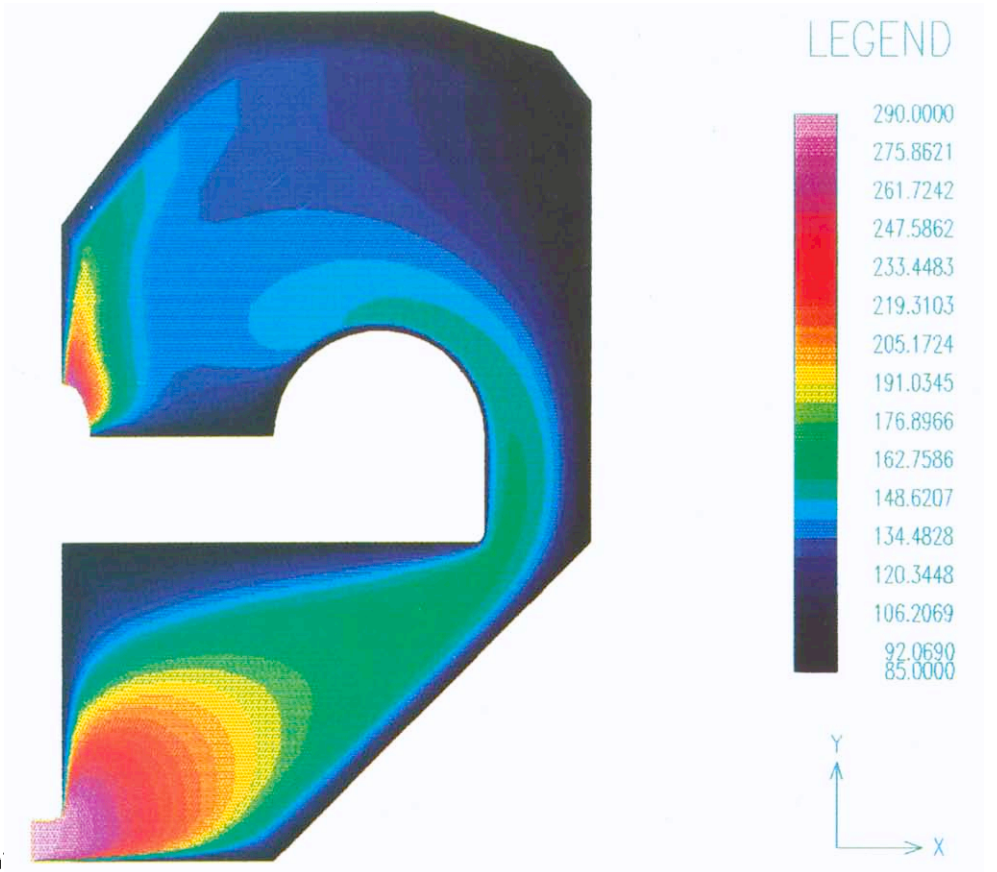

(a)

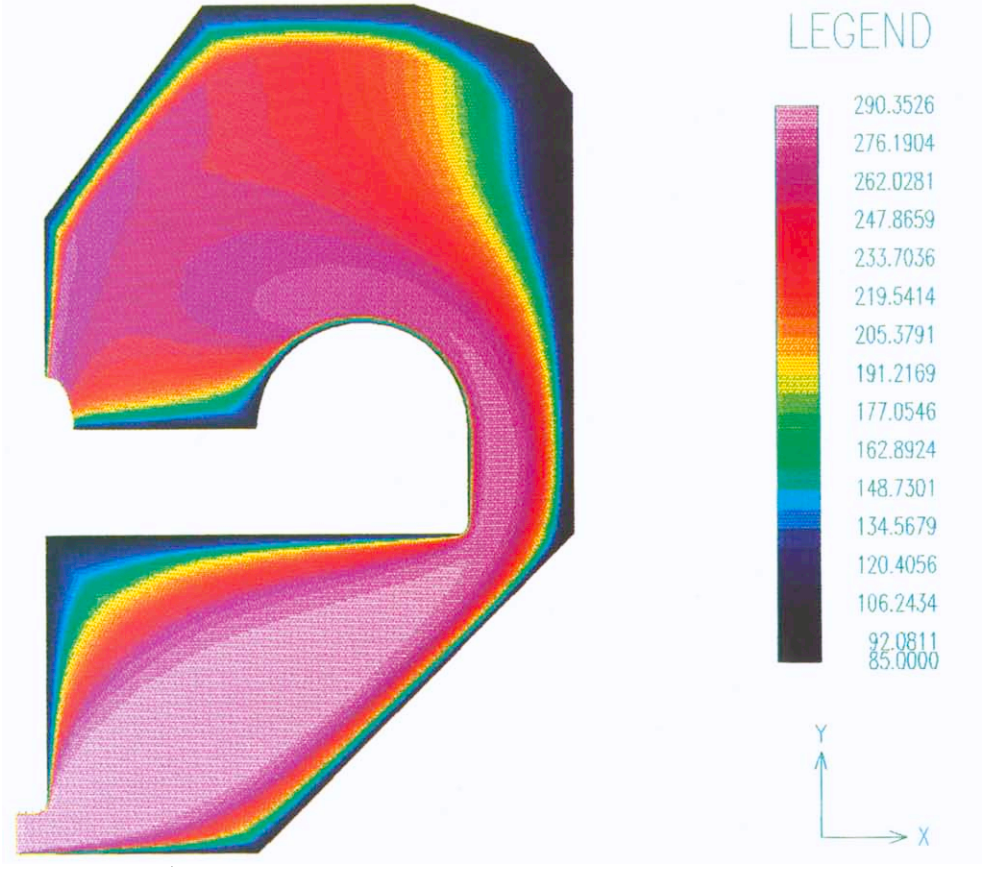

(b)

FIG. 9. Irregular mold geometry: the isotherms at three selected planes in the gap direction, $T_{inlet} = 290°C$ and $T_{wall} = 85°C$.

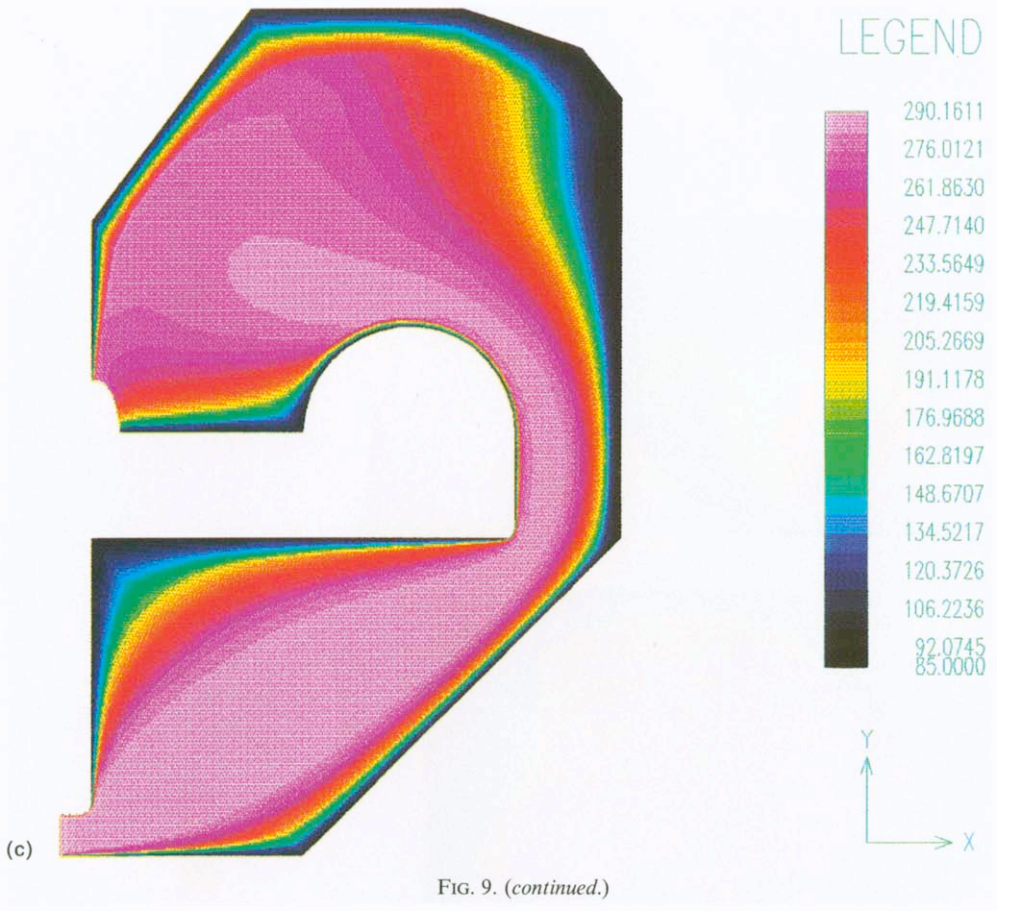

FIG. 9. (*continued.*)

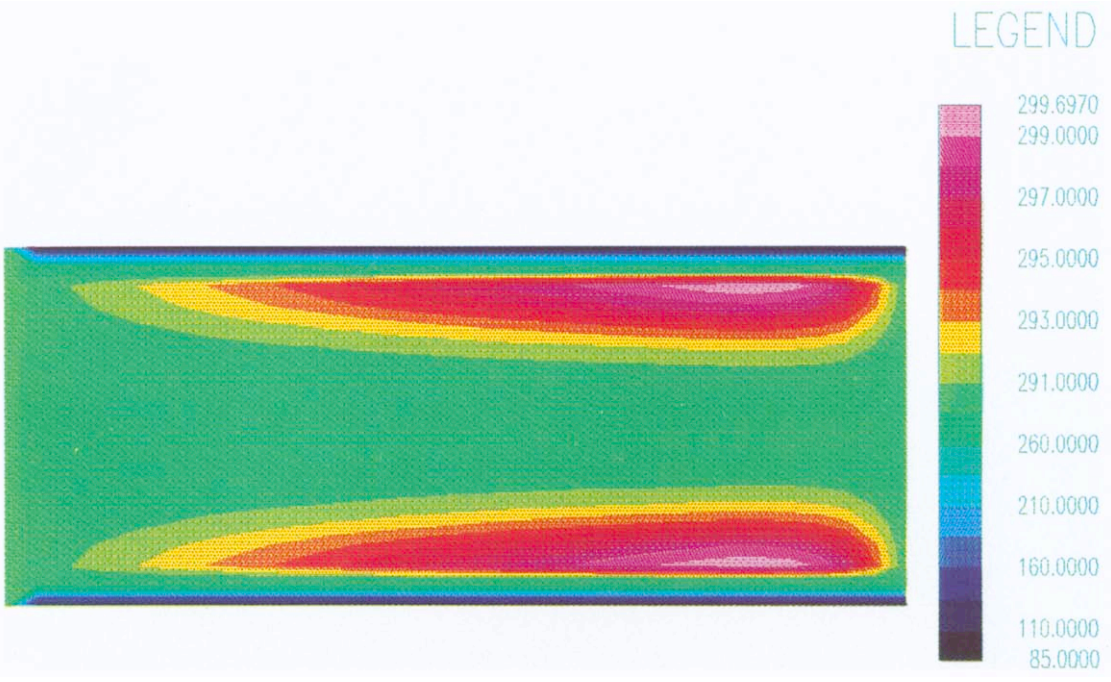

FIG. 14. The temperature distribution across the mold gapwidth for the rectangular mold cavity. The figure depicts the x–z plane with the z-direction magnified 14 times for clarity. The free surface is predicted to be at 289.988°C (T_i = 290°C and T_w = 85°C).

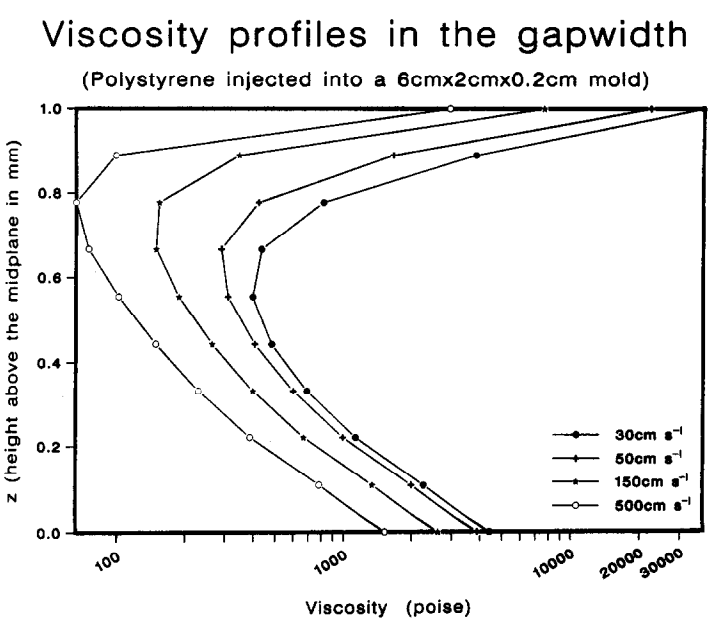

FIG. 12. The gapwise distribution of the viscosity during the filling of the rectangular mold cavity. Here, $T_0 = 453$ K and $A_n = 7.0$.

Multiply-connected mold geometries can be handled using *branch cut* or *window* approaches [26, 28, 29]. Likewise, small variations in the mold gapwidths can be analyzed by applying an algebraic transformation in the z-direction.

For injection molded parts that are three-dimensionally connected (with several protruding surfaces from a main body), the numerical grid generation approach can be extended to handle these geometries by using three-dimensional grids and independently transforming each section into a simple computational domain to solve the governing equations [37]. Such a division of parts would need only temporal information exchange at the junctions between sections when a new time cycle begins. This class of problem becomes particularly suitable for computers that have parallel processing capability, with each processor handling a particular flow zone.

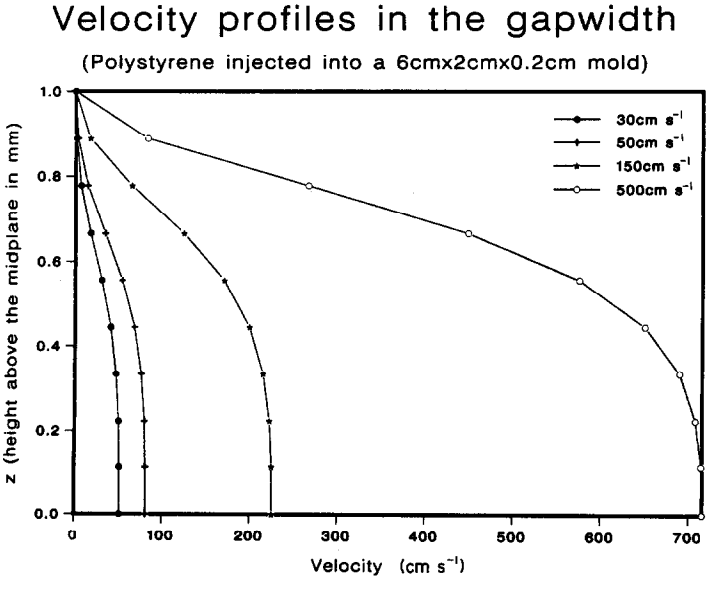

FIG. 13. The velocity profiles across the half gap for various injection speeds into the rectangular mold. The strong coupling between the temperature and velocity fields is evident.

Acknowledgements—This study was supported by the National Science Foundation through the Engineering Research Centers program. The authors would like to thank Dr P. J. Mallon and Dr M. Crochet for their helpful discussions, and Scott Gilmore for his assistance in computer graphics.

REFERENCES

1. M. R. Kamal, E. Chu, P. G. Lafleur and M. E. R. Yan, Computer simulation of injection mold filling for viscoelastic melts with fountain flow, *Polym. Engng Sci.* **26**(3), 190–196 (1986).
2. M. R. Kamal, S. K. Goyal and E. Chu, Simulation of injection mold filling of viscoelastic polymer with fountain flow, *A.I.Ch.E. Jl* **34**(1), 94–106 (1988).
3. M. R. Kamal and P. G. Lafleur, Computer simulation of injection molding, *Polym. Engng Sci.* **22**(17), 1066–1074 (1982).
4. M. R. Kamal and Y. Kuo, The fluid mechanics and heat transfer of injection mold filling of thermoplastic materials, *A.I.Ch.E. Jl* **22**(4), 661–669 (1976).
5. M. R. Kamal and S. Kenig, The injection molding of thermoplastic materials: parts 1 and 2, *Polym. Engng Sci.* **12**(4), 294–301 (1972).
6. C. A. Hieber and S. F. Shen, Flow analysis of the non-isothermal two-dimensional filling process in injection molding, *Israel J. Technol.* **16**, 248–254 (1978).
7. C. A. Hieber and S. F. Shen, A finite-element/finite-difference simulation of the injection molding filling process. *J. Non-Newtonian Fluid Mech.* **7**, 1–32 (1980).
8. A. Couniot and M. J. Crochet, Finite elements for the numerical simulation of injection molding. Presented at the Annual Technical Workshop of the Center for Composite Materials, University of Delaware, Newark, Delaware, January (1987).
9. L. Schwartz, Stability of Hele–Shaw flows: the wetting layer effect, *Physics Fluids* **29**(9), 3086–3088 (1986).
10. R. C. Givler, Numerical techniques for the prediction of flow induced orientation. Technical Report CCM-83-11, Center for Composite Materials, University of Delaware, Newark, Delaware (1983).
11. R. C. Givler, M. J. Crochet and R. B. Pipes, Numerical prediction of fiber orientation in dilute suspensions. *J. Composite Mater.* **17**(330), 330–343 (1983).
12. R. C. Givler, FIBOR, a computational code for predicting process induced fiber orientations in flows of dilute suspensions. Technical Report, Center for Composite Materials, University of Delaware, Newark, Delaware (1983).
13. S. Richardson, Hele–Shaw flows with a free boundary produced by the injection of fluid into a narrow channel, *J. Fluid Mech.* **56**(4), 609–618 (1972).
14. H. Schlichting, *Boundary-layer Theory*, Chap. VI, pp. 114–116. McGraw-Hill, New York (1968).
15. R. A. Behrens, M. J. Crochet, C. D. Denson and A. B. Metzner, Transient free-surface flows: motion of a fluid advancing in a tube, *A.I.Ch.E. Jl* **33**(7), 1178–1186 (1987).
16. D. J. Coyle, J. W. Blake and C. W. Macosko, The kinematics of fountain flow in mold-filling, *A.I.Ch.E. Jl* **33**(7), 1168–1177 (1987).
17. C. G. Gogos, C.-F. Huang and L. R. Schmidt, The process of cavity filling including the fountain flow in injection molding, *Polym. Engng Sci.* **26**(20), 1457–1466 (1986).
18. H. P. Wang, Personal communication, General Electric Co. Research and Development, Schenectady, New York (1987).
19. A. I. Isayev (Editor), Melt-viscosity characterization and its application to injection molding. In *Injection and Compression Molding Fundamentals*, p. 32. Marcel Dekker, New York (1987).
20. J. P. Coulter and S. I. Güçeri, Resin impregnation during the manufacturing of composite materials subject to prescribed injection rate, *J. Reinforced Plastics Composites* 7(3), 200–219 (1988).
21. P. J. Carreau , Ph.D. Thesis, University of Wisconsin, Madison (1968).
22. R. B. Bird, R. C. Armstrong and O. Hassager, *Dynamics of Polymeric Liquids*, Vol. 1, p. 235. Wiley, New York (1977).
23. J. F. Thompson (Editor), *Numerical Grid Generation*, Elsevier Science, Amsterdam (1982).
24. J. F. Thompson, A survey of grid generation techniques in computational fluid dynamics, AIAA 21st Aerospace Sciences Meeting, pp. 1–36 (1983).
25. J. F. Thompson, Z. V. A. Warsi and C. W. Mastin, Boundary-fitted coordinate systems for numerical solutions of partial differential equations—a review, *J. Computational Phys.* **47**, 1–108 (1982).
26. J. F. Thompson, F. C. Thames and C. W. Mastin, Automatic numerical generation of body-fitted curvilinear coordinate systems on field containing any number of arbitrary 2-dimensional bodies, *J. Computational Phys.* **15**, 299–319 (1974).
27. J. Häuser and C. Taylor, Numerical grid generation in computational fluid dynamics. In *Proc. Int. Conf. on Numerical Grid Generation*, Landshut, West Germany (1986).
28. S. I. Güçeri, Finite difference methods in polymer processing. In *Fundamentals of Computer Modelling for Polymer Processing* (Edited by C. L. Tucker). Hanser, München (1988).
29. N. R. Sottos and S. I. Güçeri, Residual and transient thermal stresses in laminated orthotropic composites. In *Numerical Grid Generation in Computational Fluid Dynamics* (Edited by J. Häuser and C. Taylor), pp. 741–753. Pineridge Press, Swansea (1986).
30. E. A. Farraye and S. I. Güçeri, Computational investigation of transient heat conduction in composite structures. Computer-aided Engineering Report 4/85, Department of Mechanical Engineering, University of Delaware, Newark, Delaware (1985).
31. D. L. Trafford, Computational analysis and simulation of the mold filling process for Hele–Shaw flows. Center for Composite Materials Report CCM-87-04, University of Delaware, Newark, Delaware 19716 (1987).
32. H. Rieger, U. Projahn and H. Beer, Analysis of the heat transport mechanisms during melting around a horizontal circular cylinder, *Int. J. Heat Mass Transfer* **25**, 137–147 (1982).
33. D. A. Anderson, J. C. Tannehill and R. H. Pletcher (Editors), *Computational Fluid Mechanics and Heat Transfer*. McGraw-Hill, New York (1984).
34. T. F. Ballenger, I.-J. Chen, J. W. Crowder, G. E. Hagler, D. C. Bogue and J. L. White, Polymer melt flow instabilities in extrusion: investigation of the mechanism and material and geometric variables. *Trans. Soc. Rheol.* **15** (1971).
35. M. J. Crochet, POLYFLOW, Technical Report, Mécanique Appliquée, Université Catholique de Louvain 1348, Louvain-la-Neuve, Belgium (1987).
36. D. L. Trafford and S. I. Güçeri, TGMOLD, a computational code for simulating the flow of polymers during injection molding. Technical Report, Center for Composite Materials, University of Delaware, Newark, Delaware (1987).
37. W. Schwarz, Elliptic grid generation system for three-dimensional configurations using Poisson's equation. In *Numerical Grid Generation in Computational Fluid Dynamics* (Edited by J. Häuser and C. Taylor), pp. 341–352. Pineridge Press, Swansea (1986).

APPENDIX: A GENERALIZED UPWIND DIFFERENCING SCHEME

Upwind differencing is needed for stable convergence in an iteration scheme if the Peclet number associated with the discretization tends towards large values. The choice of the upwind direction depends on the local relative velocity components $\bar{u}$ and $\bar{v}$. Upwind or central differencing can be performed for the first derivatives of a flow function f as follows.

In the ξ-direction

$$\bar{u}_{\xi,\mathrm{rel}} > 0: \quad \left.\frac{\partial f}{\partial \xi}\right|_{i,j} = \frac{f_{i,j} - f_{i-1,j}}{\Delta\xi} \tag{47}$$

$$\bar{u}_{\xi,\mathrm{rel}} < 0: \quad \left.\frac{\partial f}{\partial \xi}\right|_{i,j} = \frac{f_{i+1,j} - f_{i,j}}{\Delta\xi} \tag{48}$$

$$\bar{u}_{\xi,\mathrm{rel}} = 0: \quad \left.\frac{\partial f}{\partial \xi}\right|_{i,j} = \frac{f_{i+1,j} - f_{i-1,j}}{2\Delta\xi}. \tag{49}$$

In the η-direction

$$\bar{v}_{\eta,\mathrm{rel}} > 0: \quad \left.\frac{\partial f}{\partial \eta}\right|_{i,j} = \frac{f_{i,j} - f_{i,j-1}}{\Delta\eta} \tag{50}$$

$$\bar{v}_{\eta,\mathrm{rel}} < 0: \quad \left.\frac{\partial f}{\partial \eta}\right|_{i,j} = \frac{f_{i,j+1} - f_{i,j}}{\Delta\eta} \tag{51}$$

$$\bar{v}_{\eta,\mathrm{rel}} = 0: \quad \left.\frac{\partial f}{\partial \eta}\right|_{i,j} = \frac{f_{i,j+1} - f_{i,j-1}}{2\Delta\eta}. \tag{52}$$

The proper differencing can be identified by defining a quantity ε to specify the range over which central differencing is permissible. This quantity can be set equal to the critical Peclet number, $Pe = \bar{u}\Delta x/\alpha_t$, which gives the stability limit for central differencing along the x-direction. Thus, backward differencing is used for the flow variable f when $\bar{u} > \varepsilon$, central differencing when $|\bar{u}| < \varepsilon$ and forward differencing when $\bar{u} < -\varepsilon$. This is accomplished by describing a generic expression

$$\left.\frac{\partial f}{\partial x}\right|_{i,j} = \frac{Af_{i-1,j} + Bf_{i,j} + Cf_{i+1,j}}{\Delta x} \tag{53}$$

where the coefficients A, B and C are

$$A = -\frac{g+1}{2}$$

$$B = g$$

$$C = -\frac{g-1}{2}$$

with g defined as

$$g = NINT\left[\frac{\bar{u}}{|\bar{u}| + \varepsilon}\right] \tag{54}$$

(*NINT* is an intrinsic Fortran function that rounds off its argument to the nearest integer). This formulation allows the proper switching between the three types of differencing for the flow variable f, depending on the value of $\bar{u}$.

ECOULEMENT NON ISOTHERME DE POLYMERES DANS DES MOULES A CAVITE BIDIMENSIONNELLE MINCE: UNE APPROCHE PAR GENERATION DE GRILLE NUMERIQUE

Résumé—On étudie numériquement l'écoulement de polymères dans des moules plans à cavités de forme irrégulière. Les approximations d'Hele–Shaw sont utilisées pour simplifier les équations générales d'écoulement qui sont résolues dans le domaine d'écoulement en utilisant une génération de grille numérique. La nature non isotherme de l'écoulement est modélisée en incluant une viscosité fonction de la température et du taux de cisaillement. La distribution de température dans le fluide est calculée en utilisant une approche transitoire et tridimensionnelle, tandis que la prédiction de la position de la surface libre est faite avec l'approximation d'un état pseudo-stationnaire et en négligeant les termes d'inertie. Les prédictions numériques, comparées avec des résultats analytiques et des observations experimentales montrent une bonne précision. Les applications de l'approche sont démontrées à travers de nombreux exemples.

NICHT-ISOTHERME POLYMER-STRÖMUNGEN IN ZWEIDIMENSIONALE DÜNNE HOHLRAUMFORMEN: EIN NUMERISCHES RASTERGENERIERUNGS-VERFAHREN

Zusammenfassung—Es werden Polymerströmungen in flache Hohlraumformen unregelmäßiger Gestalt numerisch untersucht. Zur Vereinfachung der gebräuchlichen Strömungsgleichungen werden die Hele–Shaw-Näherungsansätze verwendet, die entlang dem unregelmäßigen Strömungsgebiet mit Hilfe eines numerisch erzeugten Rasters gelöst werden. Das thermische Ungleichgewicht, das in der Strömung herrscht, wird einschließlich einer von der Temperatur und der Scherrate abhängigen Viskosität berücksichtigt. Die Temperaturverteilung im Strömungsfeld wird mit Hilfe eines dreidimensionalen instationären Näherungsansatzes berechnet, wohingegen die Berechnung der Lage der freien Oberfläche mit Hilfe eines quasistationären Näherungsansatzes erfolgt, bei dem die Trägheits-Terme vernachlässigt werden. Es werden die berechneten Ergebnisse mit analytischen Ergebnissen verglichen. Überprüfungen mit experimentellen Daten zeigen eine gute Übereinstimmung. An verschiedenen Beispielen werden die Anwendungsmöglichkeiten des Näherungsverfahrens gezeigt.

НЕИЗОТЕРМИЧЕСКОЕ ТЕЧЕНИЕ ПОЛИМЕРОВ ПРИ ЗАПОЛНЕНИИ ДВУМЕРНЫХ ПРЕСС-ФОРМ. МЕТОД ЧИСЛЕННОГО ФОРМИРОВАНИЯ СЕТОК

Аннотация—Численно анализируется течение полимеров при заполнении гнезд пресс-форм неправильной плоской конфигурации. Общие уравнения движения упрощаются в приближении Хеле–Шоу и решаются затем численно в расчетной области течения неправильной формы с применением сеточных методов. Моделируется неизотермический характер течения, включая вязкость, зависящую от температуры и скорости сдвига. Поля скоростей и температур рассчитываются с использованием трехмерного нестационарного метода, а положение свободной поверхности определяется в квазистационарном приближении без учета инерционных членов. Численные расчеты сопоставлены с аналитическими решениями, а также экспериментальными данными и получено хорошее совпадение. На различных примерах демонстрируется практическое применение предложенного метода.